DOI: 10.1002/chem.200800408

Effects of Geometric Isomerism and Anions on the Kinetics and Mechanism of the Stepwise Formation of Long-Range DNA Interstrand Cross-Links by Dinuclear Platinum Antitumor Complexes

Junyong Zhang,[a] Donald S. Thomas,[a] Susan J. Berners-Price,*[a] and Nicholas Farrell*[b]

Abstract: Reported herein is a detailed study of the kinetics and mechanism of formation of a 1,4-GG interstrand cross-link by the dinuclear platinum anticancer compound [^{15}N][{*cis*-PtCl(NH$_3$)$_2$}$_2${μ-NH$_2$(CH$_2$)$_6$NH$_2$}]$^{2+}$ (1,1/*c*,*c* (**1**)). The reaction of [^{15}N]**1** with 5′-{d(ATAT**G**TACATAT)$_2$} (**I**) has been studied by [^{1}H,^{15}N] HSQC NMR spectroscopy in the presence of different concentrations of phosphate. In contrast with the geometric *trans* isomer (1,1/*t*,*t*), there was no evidence for an electrostatic preassociation of 1,1/*c*,*c* with the polyanionic DNA surface, and the pseudo-first-order rate constant for the aquation of [^{15}N]**1** was actually slightly higher (rather than lower) than that in the absence of DNA. When phosphate is absent, the overall rate of formation of the cross-link is quite similar for the two geometric isomers, occurring slightly faster for 1,1/*t*,*t*. A major difference in the DNA binding pathways is the observation of phosphate-bound intermediates only in the case of 1,1/*c*,*c*. 15 mM phosphate causes a dramatic slowing in the overall rate of formation of DNA interstrand cross-links due to both the slow formation and slow closure of the phosphate-bound monofunctional adduct. A comparison of the molecular models of the bifunctional adducts of the two isomers shows that helical distortion is minimal and globally the structures of the 1,4 interstrand cross-links are quite similar. The effect of carrier ligand was investigated by similar studies of the ethylenediamine derivative [^{15}N]**1-en**. A pK_a value of 5.43 was determined for the [^{15}N]1,1/*c*,*c*-en diaquated species. The rate of reaction of [^{15}N]**1-en** with duplex **I** is similar to that of 1,1/*c*,*c* and the overall conformation of the final adduct appears to be similar. The significance of these results to the development of "second-generation" polynuclear platinum clinical candidates based on the 1,1/*c*,*c* chelate (dach) series is discussed.

Keywords: antitumor agents · bioinorganic chemistry · DNA · kinetics · platinum

Introduction

The dinuclear compounds [{*trans*-PtCl(NH$_3$)$_2$}$_2${μ-NH$_2$(CH$_2$)$_n$NH$_2$}]$^{2+}$ (1,1/*t*,*t*, $n=6$) and [{*cis*-PtCl(NH$_3$)$_2$}$_2${μ-NH$_2$(CH$_2$)$_n$NH$_2$}]$^{2+}$ (1,1/*c*,*c*, $n=6$) belong to the class of multinuclear platinum am(m)ine anticancer agents that exhibit antitumor and DNA-binding properties that are significantly different to those of the mononuclear complexes based on cisplatin.[1–6] This class includes the trinuclear [{*trans*-PtCl(NH$_3$)$_2$}$_2$(μ-*trans*-Pt(NH$_3$)$_2$}{NH$_2$(CH$_2$)$_n$NH$_2$}$_2$)]$^{4+}$ (1,0,1/*t*,*t*,*t*, $n=6$, or BBR3464), which has undergone Phase II clinical trials (summarized in refs [1,7–9]). The overall charge as well as the linker flexibility and hydrogen-bonding capability of these compounds are thought to be related to their improved cytotoxic and antitumor properties relative to cisplatin and its derivatives.[10–12] Multinuclear platinum complexes react with DNA more rapidly than cisplatin and produce a different bifunctional DNA adduct profile, typified by long-range (Pt,Pt) interstrand cross-links.[13]

Many important anticancer drugs also produce covalent DNA interstrand cross-links, the formation of which is implicated in their mechanism of action.[14,15] Interstrand cross-

[a] Dr. J. Zhang, Dr. D. S. Thomas, Prof. S. J. Berners-Price
School of Biomedical, Biomolecular & Chemical Sciences
University of Western Australia, Crawley, WA, 6009 (Australia)
Fax: (+618) 6488-1005
E-mail: sue.berners-price@uwa.edu.au

[b] Prof. N. Farrell
Department of Chemistry, Virginia Commonwealth University
Richmond, Virginia, 23284-2006 (USA)
Fax: (+1) 804-828-8599
E-mail: npfarrell@vcu.edu

Supporting information for this article is available on the WWW under http://www.chemeurj.org/ or from the author.

 © 2008 Wiley-VCH Verlag GmbH & Co. KGaA, Weinheim

links are also likely to represent a particularly toxic form of spontaneous DNA damage induced by carcinogens.[15,16] In general, the repair capacity of drug-induced DNA adducts is strongly implicated in both tumor sensitivity and acquired drug resistance in tissue culture and possibly also in the clinic.[15,17,18] The interstrand cross-link, which involves covalent modification of both strands of DNA, is intrinsically more difficult to repair by nucleotide excision repair (NER), the main cellular process to remove bulky, helix-distorting DNA adducts.[15,16,19] In keeping with this understanding, structurally distinct DNA adducts of cisplatin differ in their susceptibility to DNA repair.[19–21] Cisplatin 1,3-(GpNpG) intrastrand cross-links are repaired more efficiently than the 1,2-intrastrand (GpG) adduct.[22,23] The cisplatin interstrand cross-link, however, is not repaired in the same fashion.[23] Similarly, (Pt,Pt) interstrand cross-links of BBR3464 are not as efficiently repaired as their analogous intrastrand cross-links.[24]

The inherent instability and low yields of many interstrand cross-links is a challenge to characterization by the typical enzymatic digestion/isolation route.[14] In addition, isolation of interstrand cross-links from plasmid DNA does not provide information regarding the detailed mechanism of formation and the influence of factors such as flanking sequences or the tertiary structure of the target DNA. [^{1}H,^{15}N] HSQC NMR spectroscopy is a powerful method for examining the kinetics of DNA platination reactions[25] and we have previously used this technique to examine the kinetics and mechanism of the formation of interstrand cross-links by the di- and trinuclear platinum complexes 1,1/*t*,*t* and 1,0,1/*t*,*t*,*t* (BBR3464).[26–28]

In contrast with the mononuclear examples of *cis* and *trans*-[$PtCl_2(NH_3)_2$], in the dinuclear case both geometries are antitumor active. The extent of formation of interstrand cross-links as well as local conformational distortions on DNA are affected by geometry.[1–6] The *cis* isomer (1,1/*c*,*c*) is kinetically more inert in its reactions with DNA and model nucleotides and in double-stranded DNA produces more interstrand cross-links.[1,2,13] Differences between the two geometric isomers are also manifested in their reactions with sulfur nucleophiles. When sulfur nucleophiles, such as GSH, displace the Pt–Cl bond of 1,1/*t*,*t*, *trans* labilization results in bridge cleavage and loss of the di/trinuclear structure.[29,30] This metabolic effect is likely to be highly deactivating because the capacity to form long-range cross-links is lost. Indeed, the products of BBR3464 blood metabolism may be mimicked by GSH reactions.[31] In contrast, the 1,1/*c*,*c* dinuclear structure initially remains intact upon reaction with GSH and methionine. The reactions are slower than those with the 1,1/*t*,*t* isomer, but eventually the NH_3 group *trans* to the sulfur atom is lost.[30] A unique thiolato-bridged 11-membered Pt–GS–Pt macrochelate is formed through glutathione-bridging of both platinum atoms of the same dinuclear unit.[32] Interestingly, 1,1/*c*,*c* compounds based on 1,2-diaminocyclohexane (dach) as carrier ligand show enhanced robustness in the presence of methionine, attributed to the chelate effect of the dach ring.[33]

The *cis*-oriented compounds thus represent viable "second-generation" candidates because of their enhanced robustness to sulfur nucleophiles. Any second-generation candidate should present a similar DNA-binding profile to that of the "parent" drug, in this case BBR3464. Therefore, we have initiated a detailed study of the DNA-binding of *cis*-oriented compounds. For the dinuclear 1,1/*t*,*t* complex, we were able to follow the stepwise formation of a long-range DNA 1,4-interstrand cross-link in the duplex 5′-{d(ATAT**G**TACATAT)$_2$} (**I**) by using [^{1}H,^{15}N] HSQC NMR spectroscopy and derive kinetic parameters for each step in the pathway.[26] Changes in the ^{1}H and ^{15}N shifts of the bifunctional interstrand cross-link showed evidence for the irreversible transformation of an initially formed conformer(s) into a product conformer(s). In this work we compare the kinetics of binding of the 1,1/*c*,*c* complex to the same DNA duplex. We also studied the [^{15}N]1,1/*c*,*c*-en derivative to examine the effect of the carrier ligand on the kinetics of DNA-binding. The compound is also cytotoxic at micromolar concentrations (first reported in refs. [6, 34]). Analysis of the NMR spectroscopy data in conjunction with molecular models of the mono- and bifunctional adducts provides an insight into the subtle differences in the mechanism of formation of the adducts and their structures compared with their *trans*-oriented isomers and confirms that the chelate ring does not dramatically affect the overall DNA-binding profile.

Results

The main aim of this study was to compare the stepwise formation of a 1,4-interstrand cross-link by [^{15}N]**1** with that of the analogous 1,1/*t*,*t* compound.[26] For this reason we chose to follow the platination reaction of [^{15}N]**1** with the identical self-complementary 12-mer duplex 5′-{d(ATAT**G**TACATAT)$_2$} under conditions (15 mM sodium phosphate buffer, pH 5.9, 298 K) that allow best comparison with the results of that study.[26] The use of a higher pH than that employed in the reaction of 1,1/*t*,*t* (pH 5.4) takes into account the higher pK_a of the aquated form of 1,1/*c*,*c* (6.01)[35] than 1,1/*t*,*t* (5.62),[36] so that both reactions were carried out at a pH just below the pK_a value. A higher ionic strength was used in this study, with the addition of 80 mM $NaClO_4$ required to form a stable duplex.[37]

The methodology followed that reported previously in which the stepwise formation of the cross-link was followed by [^{1}H,^{15}N] HSQC NMR spectroscopy and ^{1}H NMR spectra were also acquired to monitor oligonucleotide base pairing through examination of the imino resonances and to verify platinum-binding to guanine N7 by means of the shift of the H8 resonance from that of the unplatinated duplex.[26–28] Our previous studies of interstrand cross-linking by both 1,1/*t*,*t*[26,27] and 1,0,1/*t*,*t*,*t*[28] have shown that all the reactions follow the same sequence, with evidence for preassociation through electrostatic interactions and hydrogen bonding, aquation followed by monofunctional Pt–GN7 bond forma-

 © 2008 Wiley-VCH Verlag GmbH & Co. KGaA, Weinheim

tion, and finally fixation of the interstrand cross-link through bifunctional binding. In this case, the reactions were complicated by competing reactions involving the coordination of phosphate (Scheme 1), which were not observed previously.[26,28] Assignment of the species observed during the reactions was made by reference to our recent [^{1}H,^{15}N] HSQC NMR spectroscopy study of the aquation of [^{15}N]**1** in 15 mM phosphate buffer[35] in which several different aquated and phosphate-bound species were identified. The chemical shifts of all intermediate and bifunctional product species observed during the reaction are summarized in Table 1, representative [^{1}H,^{15}N] HSQC NMR spectra are shown in Figure 1, and plots showing changes in the aromatic and imino regions of the ^{1}H NMR spectra during the reactions are shown in Figure 2. The assignments were further verified by repeating the reaction in a higher concentration of phosphate buffer (100 mM) and in the absence of phosphate (112 mM $NaClO_4$). Representative [^{1}H,^{15}N] HSQC and ^{1}H NMR spectra from these reactions are provided in the Supporting Information.

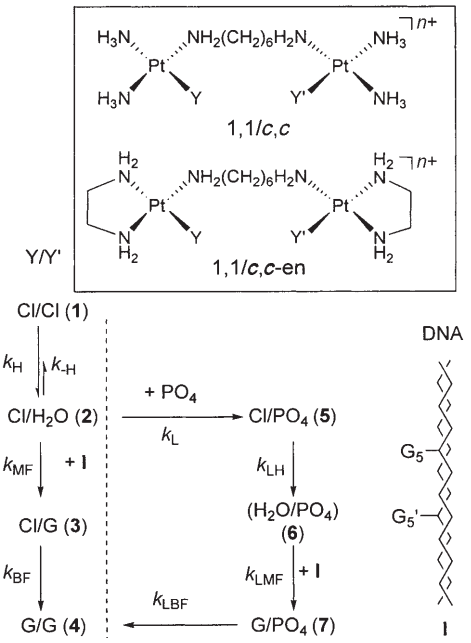

Scheme 1.

Preassociation and aquation: For the reaction of [^{15}N]**1** with **I** in 15 mM phosphate, the first [^{1}H,^{15}N] HSQC NMR spectrum was recorded 20 min after the start of the reaction. In addition to the peaks arising from [^{15}N]**1**, new peaks assignable to the {PtN_3O} group of the monoaqua monochloro species **2** are observed at $\delta = 3.89/-63.9$ (*cis*-NH_3), 4.09/−81.5 (*trans*-NH_3), and 4.58/−42.0 ppm (NH_2) (Figure 1a, see Scheme 1 and Table 1 for labeling). As for the reactions of 1,1/*t*,*t*, the signals from the {PtN_3Cl} moiety are assumed to be concealed by the signals of **1**. Surprisingly, no significant changes in the ^{1}H NMR shifts were observed for any of the peaks from **1** or **2** when compared with a control sample (no DNA added to [^{15}N]**1** in 15 mM phosphate buffer, pH 5.9). A slight difference in the ^{1}H/^{15}N NMR shifts for the *trans*-NH_3 peak of **2** could be explained by a slight difference in pH in this range close to the pK_a. This behavior is quite different to that observed for the reactions of both 1,1/*t*,*t* and 1,0,1/*t*,*t*,*t* with duplex **I**, in which the interaction with the DNA results in a comparable deshielding ($\Delta\delta = 0.05$ ppm) in the ^{1}H dimension of the signals attributed to the NH_3 (end) groups in the {PtN_3Cl} moiety of the dichloro complex and a more pronounced downfield shift ($\Delta\delta(^1H) = 0.15$–0.21 ppm) for the equivalent signals of the {PtN_3O} group of the monoaquated species. These changes were attributed to preassociation (electrostatic/hydrogen bonding) interactions between the platinum complexes and the duplex with the stronger in-

Table 1. ^{1}H and ^{15}N NMR chemical shifts [ppm] for species observed during the reaction of **1** with the self-complementary duplex 5′-{d(ATAT**G**TACATAT)$_2$} (**I**) in 15 mM phosphate at pH 5.9 (Scheme 1).[a]

1,1/*c*,*c* species[b]	$^{15}NH_3$(*cis*)[a]		$^{15}NH_3$(*trans*)[a]		$^{15}NH_2$[a]	
	$\delta(^1H)$	$\delta(^{15}N)$	$\delta(^1H)$	$\delta(^{15}N)$	$\delta(^1H)$	$\delta(^{15}N)$
1 (Cl/Cl)	3.78	−65.9	4.29	−68.4	4.48	−44.2
2a (Cl/H_2O)	[c]	[c]	[c]	[c]	[c]	[c]
2b (Cl/H_2O)	3.89	−63.9	4.09	−81.5	4.58	−42.0
3a (G/Cl)	3.65	−66.0	4.24	−68.6	4.40	−44.2
	3.69	−66.0	4.16	−68.8		
3c (G/Cl)	4.21	−62.5	4.34	−68.2	[d]	[d]
			4.42	−67.6		
4 (G/G)[e]	4.0 to 4.4	−61.7 to −64.6	4.46 to 4.65	−65.3	[d]	[d]
			4.3 to 4.45	−67.4 to 68.1		
5a (Cl/PO_4)	[c]	[c]	[c]	[c]	[c]	[c]
5d (PO_4/Cl)	3.86	−62.5	4.16	−85.7	4.67	−41.4
6b (H_2O/PO_4)[f]	[g]	[g]	4.28	−83.6	[g]	[g]
6d (PO_4/H_2O)[f]	3.86	−62.5	4.23	−85.7	4.67	−42.8
7c (G/PO_4)	[h]	[h]	[h]	[h]	[h]	[h]
7d (G/PO_4)[i]	3.86	−62.5	4.16	−85.7	4.67	−41.4
			4.10	−85.7		

[a] ^{1}H NMR chemical shifts referenced to TSP; ^{15}N chemical shifts referenced to $^{15}NH_4Cl$ (external). [b] The labels **1**–**7** refer to the complexes shown in Scheme 1 in which the ligand Y ≠ Y′ is **a** = Cl, **b** = H_2O, **c** = G N7, and **d** = PO_4. [c] The peaks for **2a** and **5a** are coincident with the peaks for **1**. [d] Concealed by the ^1H_2O peak at $\delta = \approx 4.8$ ppm. The ^{15}N shift is approximately −41.2 ppm. [e] The bifunctional adduct gives rise to broad ^{1}H,^{15}N peaks in the region indicated; sharp peaks at $\delta = 4.21/-62.5$ ppm (*cis*-NH_3) and $\delta = 4.45/-67.4$ ppm (*trans*-NH_3) account for around 30% of the total intensity. [f] Peaks for **6** were only resolved for the solution in 100 mM phosphate. The lower pH (5.4) accounts for the difference in shift for the peaks of **2b** and **6b**, which are consistent with pH titration curves.[35] [g] Peaks from the *cis*-NH_3 and -NH_2 groups of **6b** are assumed to be concealed by the peaks from **4** and the ^1H_2O peak, respectively. [h] The peaks from **7c** are concealed by the broad peaks of the bifunctional adduct **4**. [i] The peaks from **7d** and **5d** are coincident. A peak from **7d** in another monofunctionally bound phosphato species is observed in the *trans*-NH_3 region only.

© 2008 Wiley-VCH Verlag GmbH & Co. KGaA, Weinheim

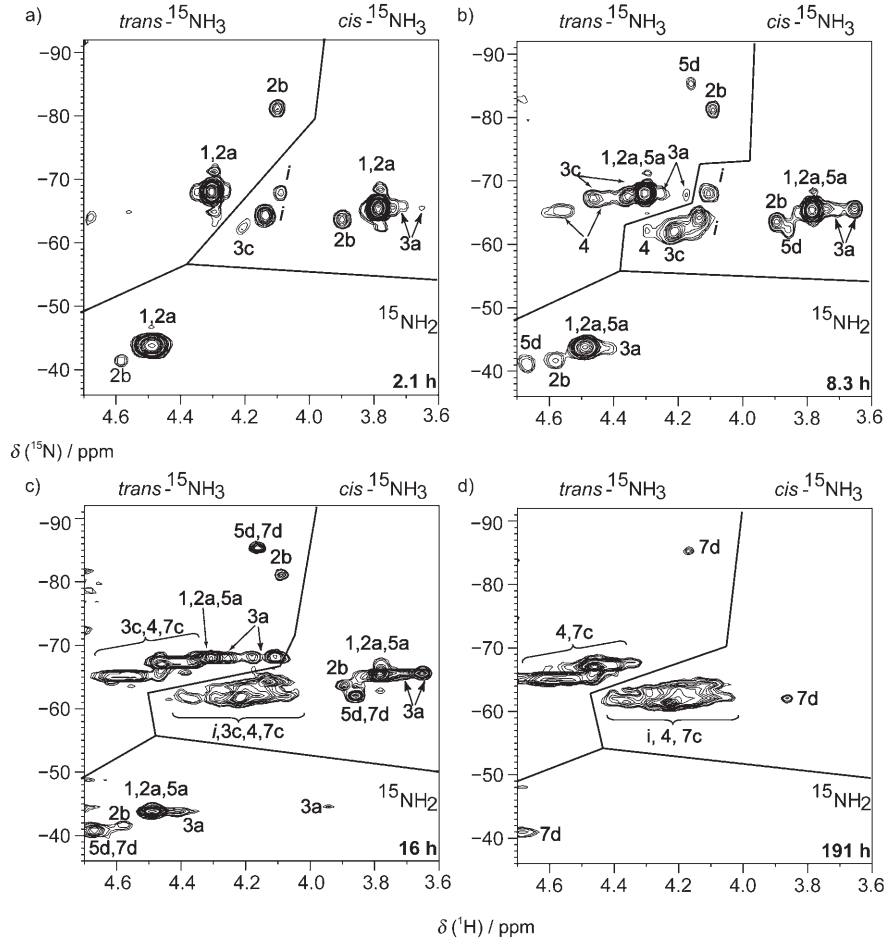

Figure 1. 2D [^{1}H,^{15}N] HSQC NMR (600 MHz) spectra at 298 K of duplex **I** in 15 mM sodium phosphate and 80 mM $NaClO_4$ after reaction with [^{15}N]**1** for the times indicated. Peaks are assigned to the *cis* and *trans* Pt–NH_3 and Pt–NH_2 groups in structures **1**–**7** in the pathways to the formation of the bifunctional adduct **4** that involve phosphate-bound intermediates (see Scheme 1 and Table 1). The labels **a**–**d** refer to species in which the ligand Y ≠ Y′ is **a** = Cl, **b** = H_2O, **c** = G N7, and **d** = PO_4; *i* = impurity in the sample of **1** (see text).

teraction observed for the aquated species consistent with the increased charge (2+). The lack of evidence for preassociation in this case could be attributable to the higher ionic strength,[37] and further experiments on 1,1/*t*,*t* under identical conditions would be required to demonstrate that the extent of preassociation differs for the two geometric isomers.

Monofunctional binding step: [^{1}H,^{15}N] HSQC peaks from the monofunctional adduct **3** were first observed after around 2 h, which is considerably later than for the reaction of 1,1/*t*,*t* under these conditions in which adduct peaks were already visible after 15 min.[26] The spectra provide evidence for at least two distinct monofunctional adducts, which are observed most clearly by the [^{1}H,^{15}N] HSQC peaks of the *cis*-NH_3 group at the unbound {PtN_3Cl} end (peaks **3a** in Figure 1). These peaks have an identical ^{15}N shift to that of [^{15}N]**1**, but are significantly shielded in the ^{1}H dimension ($\delta(\Delta\delta) = 3.65$ (−0.13) and 3.69 ppm (−0.09 ppm)). They have similar time-dependent profiles and maintain an intensity ratio of around 2:1, of which the peak at $\delta = 3.65$ ppm has the greater intensity. The time-dependent behavior of these peaks mirrors that of two peaks in the *trans*-NH_3 region (also the peaks of **3a**, see Table 1), which also have very similar ^{15}N shifts to [^{15}N]**1** and are slightly shielded in the ^{1}H dimension (δ ($\Delta\delta$) = 4.24 (−0.05) and 4.16 ppm (−0.13 ppm)). These pairs of peaks correlate with a single peak of the NH_2 group of the unbound end of **3**, which is slightly shielded with respect to [^{15}N]**1** ($\Delta\delta(^1H) = -0.08$ ppm). The observed shielding of these peaks is in complete contrast to the observations for the monofunctional adducts of both 1,1/*t*,*t*[26] and 1,0,1/*t*,*t*,*t*[28] with duplex **I** in which the Pt–NH_3 and Pt–NH_2 protons of the unbound end were slightly deshielded in comparison with the free (dichloro) complex, indicative of an electrostatic interaction between the unbound {PtN_3Cl} group and the duplex. There is also evidence for other minor monofunctionally bound species based on two very strongly shielded peaks ($\Delta\delta$ = −0.22 and −0.53 ppm) observed in the Pt–NH_2 region (δ = 4.26/−44.3 and 3.95/−44.9 ppm, Figure 1c and Figure S2c of the Supporting Information). These peaks are first observed after about 8 h, reach a maximum intensity at around 14 h, and then decrease and are no longer visible before the reaction is complete. Although these minor peaks display similar time-dependent profiles they are not of equal intensity and have slightly different ^{15}N shifts, which shows that they are not derived from a single NH_2 group of the unbound end of a monofunctional adduct. No peaks are resolved for the *cis*- or *trans*-NH_3 groups in these minor species and these are assumed to be obscured by the peaks from **1**. Peaks are identified for the *cis*- and *trans*-Pt–NH_3 groups coordinated to the guanine N7 of **I** in the monofunctional adducts (labeled **3c** in Figure 1, see Table 1). For the *cis*-Pt–NH_3 group a single peak (δ = 4.21/−62.5 ppm) is observed. The ^{1}H chemical shift is similar to that of the coordinated Pt–$(NH_3)_2$ group of the 1,1/*t*,*t* monofunctional adduct[26] and there is a similar strong deshielding ($\Delta\delta$ = 0.43 ppm) relative to the ^{1}H shift of the dichloro complex (**1**). After around 1.7 h this peak is overlapped with those of bifunctional adducts **4**. There are

 © 2008 Wiley-VCH Verlag GmbH & Co. KGaA, Weinheim

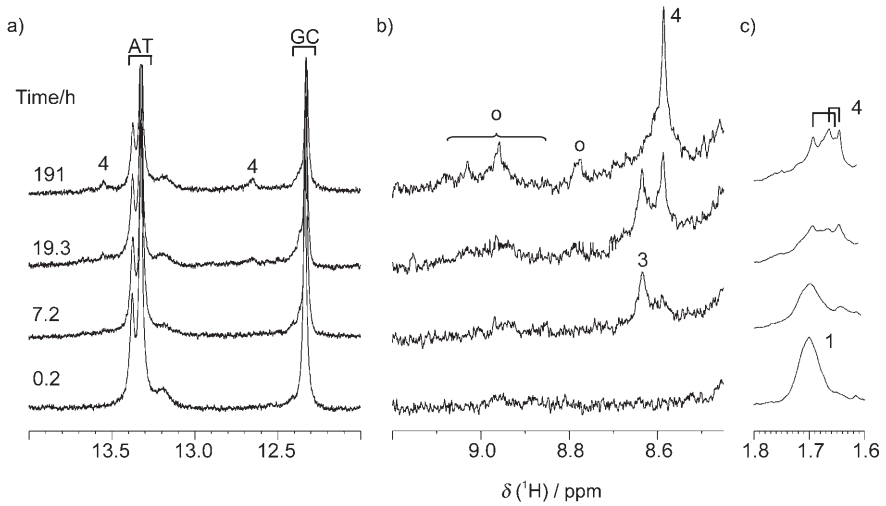

Figure 2. ^{1}H NMR spectra (600 MHz) of a) the imino and b) the aromatic regions of duplex **I** in 15 mM sodium phosphate and 80 mM $NaClO_4$ after reaction with [^{15}N]**1** for between 0 and 191 h. c) The region of the CH_2 (2 and 5) groups of the linker. In b) the peaks are assigned to the H8 resonances of the G5 (and G5′) bases coordinated to platinum in the monofunctional adduct **3** and the 1,4-interstrand cross-link **4**. Peaks labeled "o" have been assigned to other cross-linked adducts. Although the reactions are almost complete at 191 h, intense signals from unplatinated duplex are present in a) due to the excess of DNA used in the reaction.

two peaks assignable to the guanine N7-coordinated *trans*-NH_3 groups of **3**. Both are slightly deshielded ($\Delta\delta = 0.05$ and 0.13 ppm) with respect to the ^{1}H NMR shift of **1** and over time they are overlapped and obscured by peaks from the final adducts. No peaks are observed for the coordinated Pt–NH_2 group of **3** showing that these protons are strongly deshielded ($\Delta\delta \approx 0.3$ ppm) and eliminated by proximity to the $^{1}H_2O$ resonance.

In the aromatic region of the ^{1}H NMR spectrum (Figure 2b) a peak at $\delta = 8.63$ ppm is assignable to H8 of the coordinated G residue of the monofunctional adducts **3**, based on the time-dependent profile. This resonance is notably different in shift to that of the monofunctional adducts of 1,1/*t*,*t* and 1,0,1/*t*,*t*,*t* with duplex **I** ($\delta = 8.50$ and 8.48 ppm) and appears downfield (rather than upfield) of the major peak of the bifunctional adduct **4**.

When the reaction was carried out in the absence of phosphate buffer, peaks for monofunctional adducts were detected slightly earlier (ca. 1 h) in both the [^{1}H,^{15}N] HSQC (Figure S1) and the ^{1}H NMR (Figure S3a) spectra, but there was no difference in the chemical shift or number of different peaks observed for the guanine N7 bound (**3c**) and unbound ({PtN_3Cl} **3a**) groups.

Phosphate-bound intermediates: For the reaction of [^{15}N]**1** with **I** in 15 mM phosphate, [^{1}H,^{15}N] HSQC peaks assignable to the {PtN_3PO_4} group of the phosphatochloro species were first visible after around 5 h (labeled **5d** in Figure 1b). The chemical shifts for all the NH_3 and NH_2 groups are all almost identical to those observed during the aquation reaction of [^{15}N]**1** under similar conditions in the absence of DNA.[35] The partner peaks of the {PtN_3Cl} group are all concealed by the peaks of **1**. At later time points it is evident that these three peaks must also correspond to the {PtN_3PO_4} group of monofunctionally bound adduct(s) **7** because they are still visible in the spectra after peaks from the {PtN_3Cl} groups in all species (**1**, **2**, and **5**) have disappeared (Figure 1d). It is surprising that there is no difference in the chemical shift between the {PtN_3PO_4} groups in **5** and the monofunctional adduct **7**. However, a new peak ($\delta = 4.10/-85.6$ ppm) with a time-dependent profile consistent with the *trans*-NH_3 group in a second monofunctionally bound phosphato species is observed after around 19 h. The slight shielding of this peak ($\Delta\delta(^{1}H) = -0.06$ ppm) with respect to **5** is similar to that observed for the unbound end of the monofunctional G/Cl adducts relative to **1**. No similar peaks are observed for the *cis*-NH_3 and -NH_2 groups in this second G/PO_4 species and they are assumed to be overlapped by the combined peaks of **5b** and **7b**. The relative amount of the two G/PO_4 species **7** is estimated to be around 2:1, based on the intensity of the two *trans*-NH_3 peaks towards the end of the reaction when there is no overlap of the major peak with that of **5b**.

For the reaction of [^{15}N]**1** with 15 mM phosphate in the absence of DNA, the phosphatoaqua species **6** could be monitored by a distinct peak in the *trans*-NH_3 region from the {PtN_3O} moiety, with the presence of the phosphate group inducing a slightly different chemical shift to that of the aquated group of **2**, attributed to an interaction between the coordinated aqua and phosphato groups.[35] No similar peak was resolved in this reaction, which suggests that this species reacts rapidly to form the monofunctionally bound adduct **7** and never achieves a concentration high enough to be detected. Distinct peaks possibly assignable to the Pt–NH_3 groups of **6** were observed during the reaction in 100 mM phosphate, which was carried out at a slightly different pH (see Figure S2b). In neither reaction (15 or 100 mM phosphate) was a peak observed for the macrochelate phosphate-bridged species, which is recognizable by a distinct *trans*-NH_3 peak ($\delta = 4.22/-87.1$ ppm) and accounted for 25% of the species present at equilibrium for the aquation reaction of [^{15}N]**1** in 15 mM phosphate.[35]

Bifunctional adduct formation: For the reaction in 15 mM phosphate, [^{1}H,^{15}N] HSQC peaks assignable to bifunctional adducts **4** were first visible after around 4 h. Closure of the 1,4-interstrand cross-link is complete at around 200 h, compared with only 48 h for the reaction of 1,1/*t*,*t* with duplex **I**

 © 2008 Wiley-VCH Verlag GmbH & Co. KGaA, Weinheim

under comparable conditions.[26] In the absence of phosphate buffer the reaction is much faster, with peaks from **4** first visible after 2 h and the reaction complete after 50 h (Figure S1). In the *cis*-NH_3 region of the [^{1}H,^{15}N] HSQC NMR spectrum peaks from **4** first appear as a broadening around the monofunctional G/Cl peak (**3c**) that then gradually spread out in both the ^{1}H and ^{15}N dimensions. At the end of the reaction, the *cis*-NH_3 peak arising from **4** consists of around seven different overlapped peaks with the peak at the initial shift of **3c** ($\delta = 4.21/-62.5$ ppm) accounting for around 30% of the total intensity. Similarly, in the *trans*-NH_3 region one of the first peaks assignable to **4** to appear has almost an identical shift ($\delta = 4.45/-67.4$ ppm) to one of the G/Cl peaks (**3c**) and at the end of the reaction a peak at this shift accounts for around 30% of the total product. Other peaks initially appear at $\delta = 4.55/-65.4$ and $5.61/-65.3$ ppm and these peaks merge over time so that at the end of the reaction there are two broadened peaks with ^{15}N shifts centered at $\delta = -65.3$ and -67.6 ppm. Peaks arising from the NH_2 groups of **4** are largely eliminated by the suppression of the ^1H_2O, but a broadened peak ($\delta(^{15}N) = -41.2$ ppm) is observed slightly downfield of the ^1H_2O resonance (Figure S4).

In the aromatic region of the ^{1}H NMR spectrum (Figure 2b) there is a broadened peak at $\delta = 8.59$ ppm assignable to H8 protons of the platinated G residues of **4**. The chemical shift is identical to that of the 1,4-cross-link formed by 1,1/*t*,*t* with the same sequence[26] and similar also to that of the adduct of 1,0,1/*t*,*t*,*t* in which two conformers with slightly different H8 shifts ($\delta = 8.60$ and 8.58 ppm) were observed.[28] A notable difference for the reaction of [^{15}N]**1** with respect to these reactions is the appearance of a cluster of peaks in the H8 region of the ^{1}H NMR spectrum between $\delta = 8.8$ and 9.2 ppm. Although the chemical shifts of these peaks are quite similar to those previously assigned to other (cross-linked) adducts formed from the monofunctional G/Cl adducts, they account for a much larger proportion of the total product (32%) compared with the reactions with 1,1/*t*,*t* and 1,0,1/*t*,*t*,*t* (less than 10%). The ^{1}H/^{15}N peaks for these other products cannot be distinguished from those of the major cross-linked adduct in the HSQC spectra.

In the imino region (Figure 2a) there is one downfield-shifted resonance ($\delta = 13.55$ ppm) assignable to an AT base pair in the bifunctional adduct(s) and a peak at $\delta = 12.65$ ppm assignable to GH1, shifted downfield on platination. The shift is similar to that observed for the 1,1/*t*,*t* and 1,0,1/*t*,*t*,*t* cross-links.[26,28] For **1** in the absence of DNA there are three broadened multiplets that arise from the CH_2 protons of the linker: $\delta = 1.40$ (CH_2 3/4), 1.72 (CH_2 2/5), and 2.69 ppm (CH_2 1/6). On reaction with duplex **I** only the peak from the CH_2 (2/5) protons is observed in a region free from overlap. At the conclusion of the reaction two sets of peaks ($\delta = 1.65$, 1.67, and 1.66, 1.70 ppm) are observed with a relative intensity of 2:1 (Figure 2c), which are possibly attributable to the linker methylene groups 2 and 5 in two different conformers of the bifunctional adduct.

The [^{1}H,^{15}N] HSQC NMR spectra of the final products of the reactions under the three different conditions (100 mM perchlorate or 15 or 100 mM phosphate) appear identical (see Figure S4) and the ^{1}H NMR spectra show very similar peaks in the G H8 region of the ^{1}H NMR spectra (Figure S3). The important distinction is the very different times for the completion of the reactions, between 50 h (no phosphate) and 20 d (100 mM phosphate).

Kinetic analysis: For the purposes of the kinetic fits the concentrations of the species present at each time point were obtained from the relative volumes of the peaks in the *cis*-Pt–NH_3 region, after correcting for peak overlap as described below. In the absence of phosphate the reaction was analyzed by the same kinetic model (Scheme 1) as used for the reaction of 1,1/*t*,*t*.[26] The aquation process was modeled as a reversible pseudo-first-order reaction. In the absence of a competing nucleophile the aquation of **1** occurs such that the equilibrium between aquated and chloro species lies strongly towards the chloro side.[35] Once formed, the aqua chloro species **2** reacts rapidly and irreversibly with the duplex. The binding of **2** to duplex **I** was treated as an irreversible second-order reaction, first-order with respect to the concentration of both **2** and the duplex. Because no [^{1}H,^{15}N] HSQC peak was observed assignable to a monofunctional aqua species, the formation of the bifunctional cross-links (**4**) were modeled to form directly from the monofunctional adduct. This process was treated as irreversible first-order with respect to the concentration of **3**. The rate constants are listed in Table 2 and the computer best-fits for the rate constants are shown in Figure 3. The rate constant for the aquation step measured here is marginally higher than that obtained in the reaction of [^{15}N]**1** in 15 mM perchlorate in the absence of DNA. This result differs from that observed for 1,1/*t*,*t* (and 1,0,1/*t*,*t*,*t*) for which aquation of the chloro complex was slowed in the presence of DNA. On the other hand the monofunctional binding rate constant is almost identical for the reactions of both **1** and 1,1/*t*,*t*[26] with duplex **I**. The rate constants for the conversion of the monofunctional adduct **3** to the bifunctional adduct are comparable and consistent with the expected relative values of the aquation rate constants if aquation of the monofunctional adduct occurs prior to fixation of the cross-link and this step is rate-limiting.

Table 2. Rate constants for the reactions between **1** and duplex **I**.[a]

Rate constant	1,1/*c*,*c* (**1**) 112 mM ClO_4^-	1,1/*c*,*c* (**1**) 15 mM ClO_4^- (no DNA)[c]	1,1/*t*,*t*[b] 15 mM PO_4^-
k_H [10^{-5} s^{-1}]	2.99 ± 0.06	2.26 ± 0.08	4.15 ± 0.04
k_{-H} [M^{-1} s^{-1}]	0.033 ± 0.006	0.50 ± 0.02	–
k_{MF} [M^{-1} s^{-1}]	0.42 ± 0.04		0.47 ± 0.06
k_{BF} [10^{-5} s^{-1}]	3.25 ± 0.07		3.39 ± 0.04

[a] The rate constants are defined in Scheme 1. [b] Data from ref. [26]. [c] Data from ref. [35].

 © 2008 Wiley-VCH Verlag GmbH & Co. KGaA, Weinheim

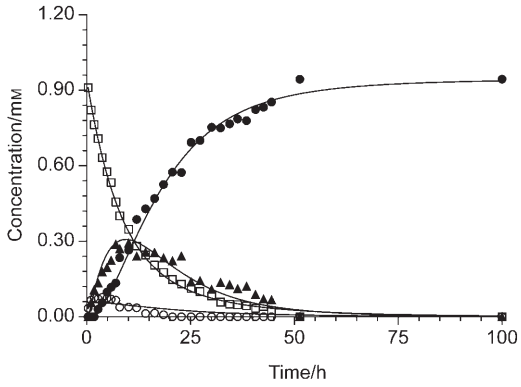

Figure 3. Plots of the relative concentrations of species observed during the formation of the 1,4-interstrand cross-link by the reaction (at 298 K) of [^{15}N]**1** with duplex **I** in 110 mM $NaClO_4$. The concentrations are based on the relative peak volumes of peaks in the *cis*-Pt−NH_3 region. The curves are computer best-fits for the rate constants shown in Table 2. Labels: **1** (Cl/Cl) □, **2** (Cl/H_2O) ○, **3** (G/Cl) ▲, **4** (G/G) ●. The time-dependent plots for the species observed during the reactions carried out in 15 mM phosphate, 80 mM $NaClO_4$, and 100 mM sodium phosphate are shown in Figure S5 of the Supporting Information.

The reactions of **1** and **I** in the presence of phosphate could not be analyzed in detail, but the time-dependent plots based on the estimated concentrations of the different species are provided in Figure S5.

Molecular models

Monofunctional adduct: A model for the monofunctional (G/Cl) adduct **3** formed from **1** and duplex **I** is shown in Figure 4a and a comparison of this model with that of the monofunctional adduct formed by the geometric isomer 1,1/*t*,*t* with the same duplex[26] is provided in the Supporting Information. To construct a model of the monofunctional adduct we first considered four different orientations of the {PtN_3} group coordinated to G5 N7 in which either the *cis*-NH_3 or -NH_2 groups are hydrogen bonded to G O6 and the amine linker lies either 3′ or 5′ to the G5 plane (Scheme 2).

We attempted to model all four conformers, but found that the two orientations (**C** and **D**) with the amine linker group below the G5 plane were unstable during the minimization and reorientated to a position above the plane of G5. The two above-plane orientations (**A** and **B**) are illustrated in the models of the bifunctional adduct (see below). The monofunctional adduct shown in Figure 4a was constructed by using orientation **A** as the starting point and shows hydrogen-bonding interactions that are largely consistent with the NMR data, as discussed below. For the {PtN_3} unit coordinated to the N7 atom of G5* an NH_3···O6 hydrogen bond is observed between the *cis*-NH_3 group and the O6 of that guanine (H···O6 distance = 2.5 Å). An additional hydrogen bond is observed from an ammine hydrogen of this group

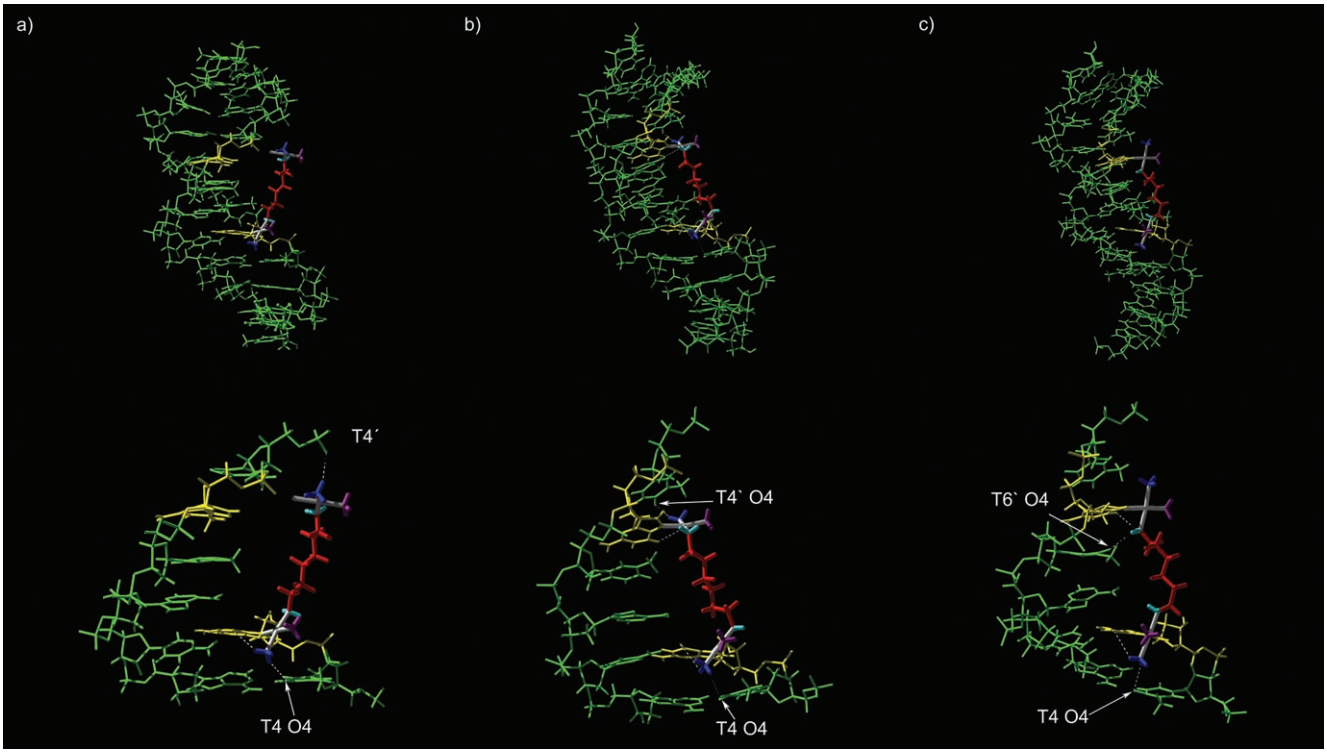

Figure 4. Molecular models of a) the monofunctional adduct and b,c) two conformers of the bifunctional 1,4-interstrand cross-link formed by **1** and duplex **I** with close-up views showing the hydrogen bonding between the Pt−NH_3 and Pt−NH_2 groups and the duplex (in white): **I** (green), guanine G5* and G5′ (yellow), −$(CH_2)_6$− linker of **1** (red), NH_2 groups (pale blue), *trans*-NH_3 groups (purple), *cis*-NH_3 groups (dark blue). Bases not involved in the interactions have been omitted from the close-up views for clarity. A figure showing a comparison of these models with those of the mono- and bifunctional adducts of 1,1/*t*,*t* (ref. [26]) are provided in the Supporting Information.

 © 2008 Wiley-VCH Verlag GmbH & Co. KGaA, Weinheim

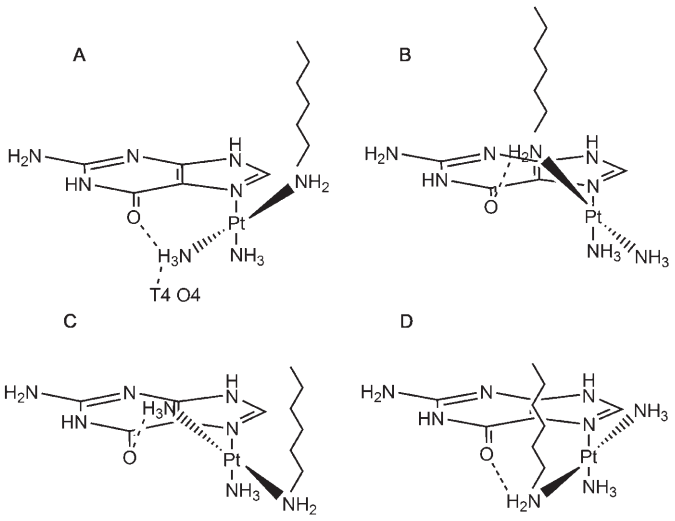

Scheme 2. The four different orientations for the $\{PtN_3\}$ group of **1** bound to guanine N7.

and O4 of the adjacent thymine (T4) residue (distance = 2.1 Å). The environment of the *cis*-NH_3 group is similar to that of one of the Pt–NH_3 groups of the bound end of the 1,1/*t*,*t* monofunctional adduct, which is hydrogen bonded to O6 of G5* (see Figure S6). In the latter case the other Pt–NH_3 group (equivalent to the NH_2 group of 1,1/*c*,*c*) points towards the phosphate backbone, which allows the formation of a short (distance = 2 Å) hydrogen bond with a phosphate oxygen. The NH_2 group in the 1,1/*c*,*c* adduct is too far from the phosphate backbone to form a hydrogen bond with a phosphate oxygen (distance = 6.5 Å) and lies closer to the O4 of T6 (distance = 4.4 Å). The *trans*-NH_3 group (equivalent to the NH_2 group in the 1,1/*t*,*t*) points away from the major groove and makes no contacts other than with the solvent. Significant differences are observed for the unbound $\{PtN_3Cl\}$ end of the monofunctional adducts of the two geometric isomers. For the 1,1/*t*,*t* adduct the unbound end interacts with the phosphate backbone facilitated by the orientation of the two NH_3 groups with hydrogen bonds observed between a proton from each ammine group and two different phosphate oxygen atoms (distance = 1.8 Å). In contrast, the molecular dynamics simulations of the 1,1/*c*,*c* monofunctional adduct show considerable flexibility for the unbound end, which is seen to move in and out of the major groove during the simulation. The model depicted in Figure 4a shows a single hydrogen bond with the phosphate backbone between a proton of *cis*-NH_3 and the phosphate oxygen atom of T4 (distance = 2.3 Å).

Bifunctional adduct: Two possible models for the bifunctional 1,4-interstrand cross-link formed by **1** and **I** in B-form DNA are shown in Figure 4b and c, and these are compared with the previously reported model of the 1,1/*t*,*t* cross-link in Figure S7. The models were constructed by using the monofunctional adduct as the starting point so that both show the same orientation for the $\{PtN_3\}$ group coordinated to G5*, but have different orientations (**A** and **B**) for the other group coordinated to G5′. As was found for the model of the bifunctional adduct formed by 1,1/*t*,*t*, the flexibility and length of the linker group do not force the helix to bend to accommodate the formation of the cross-links in either case. For both models the hydrogen-bonding interactions for the $\{PtN_3\}$ group bound to G5* N7 are essentially the same as those observed for the monofunctional adduct with two NH···O hydrogen bonds from the *cis*-NH_3 group to G5 O6 and T4 O4. The orientation of the NH_2 group differs in the two cases (pointing towards either the major groove or phosphate backbone), but in neither case are hydrogen bonds observed. The model in Figure 4b shows similar hydrogen-bonding interactions for the $\{PtN_3\}$ group bound to G5′, with two NH···O hydrogen bonds for the *cis*-NH_3 group (with O6 of G5′ and O4 of T4′) and the NH_2 protons positioned some 4.5–5.5 Å from the nearest oxygen atom (either a phosphate oxygen atom or T6′ O4). In the alternative model (Figure 4c) there is a hydrogen bond between an amine proton of the NH_2 group and G5′ O6 (distance = 2.7 Å) and the *cis*-NH_3 group points towards the phosphate backbone, but the distance (> 5 Å) is too great to form a hydrogen bond. Comparison of these models with those of the bifunctional adducts of 1,1/*t*,*t* (Figure S7) shows that helical distortion is minimal and globally the structures of the cross-links are quite similar. The key difference is the greater steric constraints for the $-(CH_2)_6-$ chain, which lies much closer to the DNA in the 1,1/*c*,*c* case because the NH_2 group is *cis* to the site of platination. The models for both conformers of the bifunctional adduct show several close interactions between the linker methylene hydrogen atoms and the thymine methyl groups, and these are different in the two cases. In Figure 4b there are close contacts (2.3–2.6 Å) for methylene groups 2 and 3 (with T6 CH_3) and 6 (with T6′ CH_3). In the second conformer (Figure 4c) there is one short contact (2.3 Å) for methylene group 3 (with T6 CH_3) and a slightly longer distance (2.8 Å) between methylene groups 5 and T6′ CH_3. On the other hand, the model of the bifunctional adduct of 1,1/*t*,*t* (Figure S7) shows that all methylene linker hydrogen atoms are at distances of at least 3.4 Å from the closest atom on the DNA.

Comparison with 1,1/*c*,*c*-en: To examine the effect of the carrier ligand we first examined the pK_a values of the coordinated water ligands of the [^{15}N]1,1/*c*,*c*-en diaquated species. The pH dependences of the ^{1}H and ^{15}N NMR shifts of the three NH_2 groups are shown in Figure 5. The three ^{1}H NMR titration curves were fitted to Equation (1) (see the Experimental Section) to give a pK_a value of 5.43 ± 0.04. This value is more similar to that of 1,1/*t*,*t* (pK_a = 5.62)[36] than 1,1/*c*,*c* (6.01),[35] and the difference may reflect the difference of a primary amine rather than NH_3 *trans* to the aqua ligand. The aquation rate constant for 1,1/*c*,*c*-en appears higher than that of 1,1/*c*,*c*, but is still lower than that of 1,1/*t*,*t* (see the Supporting Information).

We then used a combination of ^{1}H NMR and [^{1}H,^{15}N] HSQC NMR methods to follow the platination of

 © 2008 Wiley-VCH Verlag GmbH & Co. KGaA, Weinheim

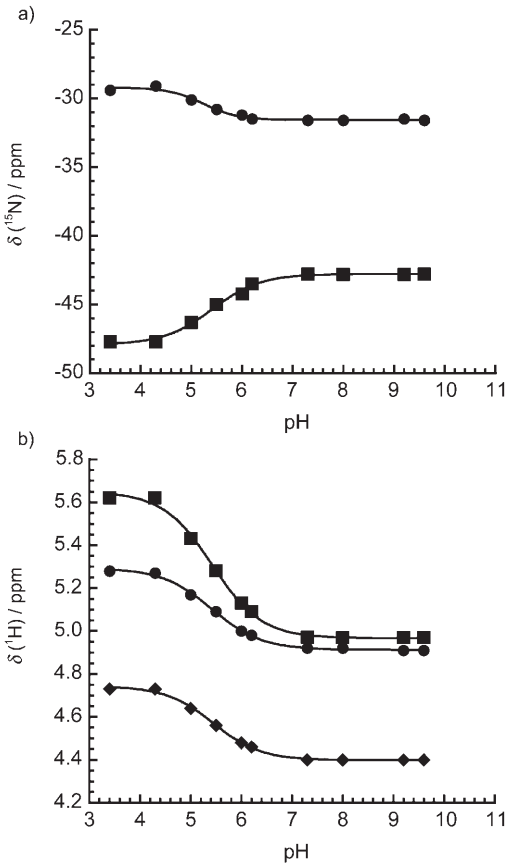

Figure 5. Plots of a) ^{15}N and b) ^{1}H chemical shifts versus pH for the Pt–NH_2 groups (*cis* (●), *trans* (■), linker (◆) in the 1,1/*c*,*c*-en diaqua complex in 100 mM $NaClO_4$ at 298 K. The pK_a values obtained are a) *cis*-NH_2 5.24 ± 0.09, *trans*-NH_2 5.41 ± 0.07; b) *cis*-NH_2 5.42 ± 0.04, *trans*-NH_2 5.42 ± 0.05, linker-NH_2 5.44 ± 0.04.

duplex **I** by [^{15}N]**1-en** at 298 K in 100 mM $NaClO_4$ at pH 5.3. The [^{1}H,^{15}N] HSQC peaks from the *cis*- and *trans*-NH_2 groups in 1,1/*c*,*c*-en are much broader than those of the *cis*- and *trans*-NH_3 groups in 1,1/*c*,*c* and the lower resolution precluded a detailed analysis of the stepwise formation of the 1,4-interstrand cross-link. Peaks from the monoaqua monochloro species **2-en** were not detectable for any of the Pt–NH_2 groups and the peaks from the GN7-bound mono- (**3-en**) and bifunctional adducts (**4-en**) could not be distinguished in either of the ethylenediamine *cis*- or *trans*-NH_2 regions. The chemical shifts of all intermediate and bifunctional product species observed during the reaction are summarized in Table 3 and representative [^{1}H,^{15}N] HSQC spectra are shown in Figure S10. The spectra show clear similarities in the reaction profile to 1,1/*c*,*c*. Notably the peaks from the linker NH_2 group coordinated to the guanine N7 in the mono- and bifunctional adducts exhibit similar strong deshielding and are obscured by proximity to the $^{1}H_2O$ resonance. A peak arising from the NH_2 group of the unbound {PtN_3Cl} end of **3-en** is observed slightly shielded with respect to [^{15}N]**1-en** ($\Delta\delta(^{1}H) = -0.07$ ppm) and the [^{1}H,^{15}N] HSQC peaks from the *cis*- and *trans*-NH_2 groups in the final product resemble those of the analogous *cis*- and *trans*-NH_3 peaks in the reaction of 1,1/*c*,*c*, with a similar spread of peaks in both ^{1}H and ^{15}N dimensions.

The ^{1}H NMR spectra (Figure 6) further show that reaction of 1,1/*c*,*c*-en with duplex **I** has a similar profile to that of 1,1/*c*,*c* under similar conditions (pH just below the pK_a of the aquated species). The rate of reaction appears to be similar and the overall conformation of the final adduct appears to be similar based on the similarity of the ^{1}H NMR imino resonances. There is one major H8 peak with a similar shift ($\delta = 8.57$ ppm), although there appears to be a much greater proportion of other side-products (ca. 56%), based on the additional peaks observed in the H8 region.

Discussion

Kinetics of formation of the 1,4-interstrand cross-link: Previous studies using other techniques have shown that 1,1/*t*,*t* compounds bind to DNA more readily than 1,1/*c*,*c* compounds[5] and the first objective of the current study was to compare the kinetics of the stepwise formation of 1,4-interstrand cross-links by the geometric isomers 1,1/*c*,*c* and 1,1/*t*,*t*. Therefore, the initial reactions of **1** with duplex **I** were carried out under similar conditions to those employed in our previous study of 1,1/*t*,*t* in the presence of 15 mM phosphate buffer and with the chosen pH approximately 0.2 pH units below the pK_a value of the diaquated species.[26] A major difference in the DNA-binding pathways is the observation of phosphate-bound intermediates only in the case of 1,1/*c*,*c*. This difference is not simply a reflection of the greater concentration of HPO_4^{2-} present at the higher pH (5.9 vs. 5.4), because phosphate bound species were also observed

Table 3. ^{1}H and ^{15}N NMR chemical shifts for the [^{15}N]1,1/*c*,*c*-en species.

1,1/*c*,*c*-en species[a]	en-$^{15}NH_2$(*cis*)[b]		en-$^{15}NH_2$(*trans*)[b]		$^{15}NH_2$(linker)[b]	
	$\delta(^{1}H)$	$\delta(^{15}N)$	$\delta(^{1}H)$	$\delta(^{15}N)$	$\delta(^{1}H)$	$\delta(^{15}N)$
1 (Cl/Cl)	5.01	−30.8	5.47	−30.9	4.48	−43.5
2a (Cl/H(OH))	[c]	[c]	[c]	[c]	[c]	[c]
2b (Cl/H_2O)[d]	5.28	−29.4	5.62	−47.7	4.73	−40.7
(Cl/OH)[d]	4.92	−31.6	4.97	−42.8	4.40	−40.7
μ-OH[e]	5.32	−27.3	5.34	−46.2	4.62	−39.4
3a (G/Cl)	[f]	[f]	5.38	−31.1	4.42	−43.4
3c, 4 (G/Y) (Y = Cl or G)	5.30–5.54	−27.9	5.40–5.86	−31.4	[g]	[g]
	5.24–5.76	−26.6	5.55–5.98	−29.4		

[a] The labels **1**–**4** refer to the complexes shown in Scheme 1 in which the ligand Y ≠ Y′ is **a**, Cl; **b**, H_2O; **c**, G N7. [b] ^{1}H referenced to TSP; ^{15}N referenced to $^{15}NH_4Cl$ (external). [c] The peaks are coincident with the peaks of the Cl/Cl species. [d] Based on fitting pH titration curves for H_2O/H_2O species (Figure 5). [e] Hydroxo-bridged macrochelate species observed only in solutions of the diaqua species. [f] Possible resonances shielded with respect to the Cl/Cl species would be too close to the $^{1}H_2O$ signal to observe. [g] Concealed by the $^{1}H_2O$ peak at $\delta \approx 4.8$ ppm. The ^{15}N shift is around −40.6 ppm.

© 2008 Wiley-VCH Verlag GmbH & Co. KGaA, Weinheim

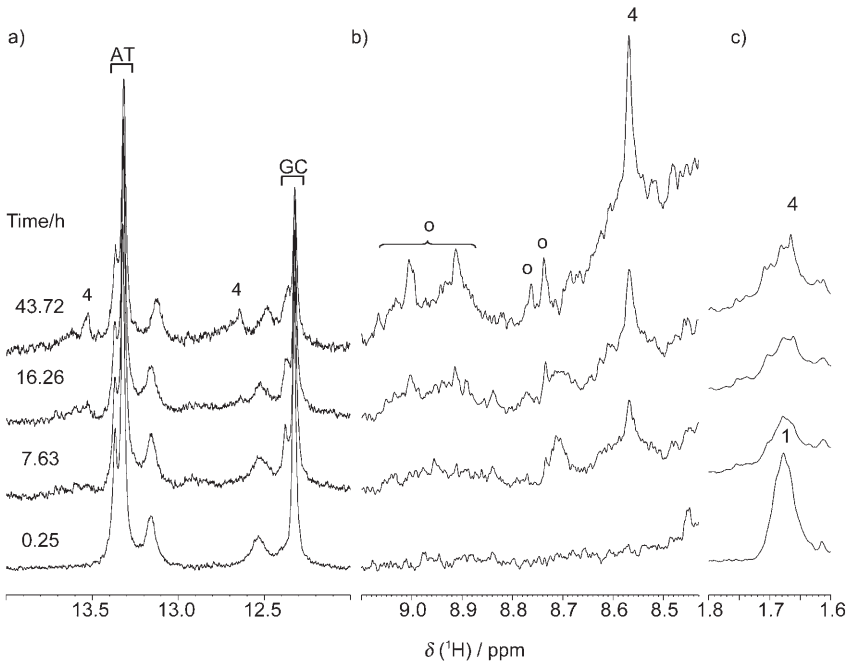

Figure 6. ^{1}H NMR spectra (600 MHz) of the imino (a) and aromatic (b) regions of duplex **I** in 15 mM sodium phosphate, 80 mM $NaClO_4$, after reaction with [^{15}N]**1-en** for between 0 and 44 h; c) shows the region of the CH_2 (2 and 5) groups of the linker. The assignments are the same as in Figure 2 for the analogous reaction with [^{15}N]**1**.

(albeit to a lesser extent) when the reaction was carried out at pH 5.2.[37] A similar dependence on geometric isomerism was found in studies of the aquation reactions in the presence of phosphate buffer. Equilibrium conditions were reached much more slowly for 1,1/*c*,*c* and a greater proportion of phosphate-bound species were present, attributable to the reduced lability of the bound phosphate (a consequence of the formation of a macrochelate phosphate-bridged species). It is evident that the presence of phosphate causes a dramatic slowing in the overall rate of formation of DNA interstrand cross-links by 1,1/*c*,*c*, and the reaction profile (Figure S5) shows that this is a consequence of both the slow formation and slow closure of the phosphate-bound monofunctional adduct. Adduct formation between cationic reagents and DNA is facilitated by the preassociation of the cations to the negatively charged surface of the polymer. Apart from the slow displacement of bound phosphate, DNA-binding will be inhibited for the 1,1/*c*,*c* phosphato species due to the reduction in charge relative to the positively charged chloro or aqua species, which are attracted to the polyanionic DNA by electrostatic interactions. Recent studies by Lippard and co-workers[38] have demonstrated that phosphate inhibits binding of cisplatin to DNA through the formation of neutral or anionic phosphato species. Further, it has been shown that the rate of platination in single-stranded DNA is controlled by a combination of access to preassociation sites and local accumulation in the vicinity of guanine N7.[39] Medium effects are also a characteristic feature of reactivity profiles for the platination of phosphorothioate-containing oligonucleotides.[40] The results presented herein contribute to the description of these effects, but unusually, in a geometry-dependent fashion. The use of [^{1}H,^{15}N] HSQC NMR spectroscopy facilitates these observations in a direct manner and indirect assessments by using salt concentration or phosphorothioate substitution are unnecessary. Thus, the details of interstrand cross-link formation for any species may present subtle differences depending on the chemical entity.

To compare the kinetics of the formation of 1,4-interstrand cross-links by **1** and 1,1/*t*,*t* with duplex **I** we repeated the reaction at a similar pH in 100 mM perchlorate. In the absence of phosphate the overall rate of formation of the cross-link is quite similar for the two reactions, occurring slightly faster for 1,1/*t*,*t*. Comparison of the individual steps of the reaction reveals some interesting differences for the two geometric isomers. For 1,1/*t*,*t*, the first step is an electrostatic interaction of the dipositive compound with the polyanionic DNA surface, as evidenced by a significant shielding of the Pt–NH_3 and Pt–NH_2 protons. This electrostatic preassociation has a strong influence on the aquation step, with the aquation rate constant significantly lowered in the presence of DNA. A similar slowing of the aquation of 1,0,1/*t*,*t*,*t*[28] and also of cisplatin[41] has been observed and attributed to the restricted access of the solvent to the platinum coordination sphere. For 1,1/*c*,*c* there is no evidence of an electrostatic preassociation between the {PtN_3Cl} groups and DNA, and consistent with this result, no lowering of the aquation rate constant is observed. In fact, the pseudo-first-order rate constant for the aquation of [^{15}N]**1** was actually higher in the presence of DNA (Table 2). This result is surprising given that 1,1/*c*,*c* and 1,1/*t*,*t* carry the same charge (2+) and, as pointed out above, the differences could reflect the differences in ionic strength in these experiments. However, the differences can be rationalized by inspection of the molecular models of the unbound {PtN_3Cl} ends of the two monofunctional adducts, as discussed below.

The rate constants for the monofunctional binding step are almost identical for 1,1/*c*,*c* and 1,1/*t*,*t*, and the rate constants for the closure step to form the interstrand cross-links are also very similar and consistent with aquation of the monofunctional adducts being rate-limiting. Overall, these results show that the slower reaction of 1,1/*c*,*c* with DNA is

 © 2008 Wiley-VCH Verlag GmbH & Co. KGaA, Weinheim

a consequence of the reduced aquation rate constant in comparison with 1,1/*t*,*t*. In the absence of DNA there is a two-fold difference in these values, but this difference reduces to 1.4-fold in the DNA-binding reactions because electrostatic preassociation has a strong influence only for the 1,1/*t*,*t* complex. Studies comparing the binding of the geometric isomers with DNA have previously shown that 1,1/*c*,*c* complexes bind to DNA at a similar rate as cisplatin but much less readily than 1,1/*t*,*t* counterparts (half-times of binding = 120 (cisplatin), 40 (1,1/*t*,*t*), and 120 min (1,1/*c*,*c*)).[13] Our results suggest that the reaction conditions will have a profound influence on the differential binding affinities of the geometric isomers. Apart from interactions with buffer components, the pH of the solution is an important factor. The pK_a value of 1,1/*c*,*c* is 0.4 units higher than that of 1,1/*t*,*t*, so a greater proportion of the more reactive aqua species will exist around physiological pH.

Structures of the mono- and bifunctional adducts: For the monofunctional adduct of 1,1/*t*,*t*, the molecular model (Figure S6) shows hydrogen-bonding interactions between the Pt–NH_3 groups and DNA that are consistent with the shift changes seen in the [^{1}H,^{15}N] HSQC NMR spectra.[26] For the Pt–$(NH_3)_2$ groups bound to N7 of G5, the two ammines can form hydrogen bonds to guanine O6 and a phosphate oxygen atom, and in this orientation the $-(CH_2)_6-$ chain is positioned so that the two NH_3 groups at the unbound end form hydrogen bonds with the phosphate backbone. This situation may reflect the transient formation of "phosphate clamps" in solution in which two *cis*-oriented NH_3 groups and a linker NH_2 (or in this case the two NH_3 groups) form a well-defined hydrogen-bonding network with a phosphate oxygen.[42] This interaction places the uncoordinated {PtN_3Cl} close to the position of guanine (G5′) on the complementary strand, which assists the formation of the 1,4-interstrand cross-link. The different geometry of 1,1/*c*,*c* leads to a greater diversity in the possible orientation of the {PtN_3} group bound to guanine N7 (Scheme 2). The NMR data for the monofunctional adduct **3** are largely consistent with the hydrogen-bonding interactions observed in the model (Figure 4a) in which the *cis*-NH_3 groups are hydrogen bonded to guanine O6 and the amine linker lies 3′ to the G5 plane. Only a single peak ($\delta = 4.21/-62.5$ ppm) is observed for the *cis*-NH_3 group on the platinum bound to DNA and the strong deshielding in the ^{1}H dimension is indicative of a strong hydrogen-bonding interaction. This behavior is similar to that observed for the Pt$(NH_3)_2$ groups in the 1,1/*t*,*t* monofunctional adduct, which exist in a similar environment, hydrogen bonded to the O6 of G5. In the latter case free rotation will produce an average of the two environments, hydrogen bonded to guanine O6 and phosphate without changing the position of the linker. For 1,1/*c*,*c*, an alternative orientation retains the *cis*-NH_3···O6 hydrogen bond, but with the amine linker on the opposite (5′) side of the G5 plane (Scheme 2**C**), but this conformer appears less favorable on the basis of the modeling data. There is a difference of about 4.5 Å for the two positions of the NH_2 group above and below the guanine plane and the 1,4-interstrand cross-link could not form in the second case because the distance is too great for platination of the G5′ residue by the uncoordinated {PtN_3Cl} group. The greater diversity of the binding modes for 1,1/*c*,*c* is a possible explanation for the higher percentage of other products observed here relative to the reactions of 1,1/*t*,*t*[26] and 1,0,1/*t*,*t*,*t*[28] with the same duplex. It may also explain the observations from previous DNA-binding studies that showed that the population of cross-linked structures is more diverse for 1,1/*c*,*c* than for the 1,1/*t*,*t* isomer.[13] Transcription-mapping experiments with natural DNA indicate that A residues are involved in minor non-interstrand adducts[13] and that DNA interstrand cross-links formed between G and complementary C residues are also possible, but not a frequent adduct in natural DNA. The NMR data provide evidence for very different environments of the uncoordinated {PtN_3Cl} groups in the monofunctional adducts of the geometric isomers. The model shown in Figure 4a does not provide any insight into why two sets of [^{1}H,^{15}N] HSQC resonances are observed for the *cis*- and *trans*-NH_3 and -NH_2 groups, which are all slightly shielded in the ^{1}H dimension with respect to those of **1**. It is evident, however, that the strong hydrogen-bonding interactions with the backbone, which lead to the deshielding of the ammine resonances of the 1,1/*t*,*t* adduct, do not occur and the observed shielding is consistent with the location of the {PtN_3Cl} group close to DNA where it is sheltered from the aqueous environment. It is possible to envisage that with one end of the molecule tethered to the DNA, the unbound {PtN_3Cl} group could approach the guanine N7 with different orientations that lead to two different conformations of the bifunctional adduct in which either the *cis*-NH_3 or NH_2 groups form a hydrogen bond to the G5′ O6. These two possibilities are illustrated in the models shown in Figure 4b and c and provide a possible explanation for the observation of two sets of NMR resonances for the unbound {PtN_3Cl} group as intermediates in the pathways to these two conformers. The models show that the linker methylene protons are located in slightly different environments in the two conformers, which is consistent with the observation of two sets of resonances (in the same 2:1 ratio) for the linker methylene groups 2 and 5 (Figure 2c). The strong deshielding observed for some NH_2 environments in the final product (^{1}H NMR shifts downfield of the ^1H_2O resonance, Figure S4) is consistent with the hydrogen-bonding interactions observed in Figure 4c. There is only one resonance (albeit broadened) assignable to H8 protons of the platinated G residues of the 1,4-interstrand cross-link, indicative of one predominant conformer, but given that the chemical shift is identical to that found for the 1,1/*t*,*t* isomer it may not be that sensitive to the different orientations of the PtN_4 plane. The similarity in the chemical shifts of the guanine H8 signals, as well as those of the shifted imino resonances, indicate that local structural perturbations of the 1,4-interstrand cross-links of the geometric isomers are quite similar. The most significant difference between the structures of the 1,4-interstrand cross-links is in the location of the methylene

 © 2008 Wiley-VCH Verlag GmbH & Co. KGaA, Weinheim

linker, which lies much closer to the DNA in the 1,1/*c*,*c* case because the diamine linker is *cis* (rather than *trans*) to the site of platination. Steric constraints imposed by the *cis* position of the diamine linker could affect protein recognition and DNA repair in manners different to the 1,1/*t*,*t* counterparts.[5,6,43]

Finally, a notable feature of the reaction of 1,1/*t*,*t* with duplex **I** was the gradual and irreversible transformation of [^{1}H,^{15}N] HSQC peaks in the Pt–NH_2 region as the initially formed conformer was converted into product conformer(s).[26] Similar behavior was observed for both the 1,4- and 1,6-interstrand cross-links formed by 1,0,1/*t*,*t*,*t*[28] and we speculated that the changes could be indicative of a B→Z conformational change, as has been demonstrated to occur in poly(dG-dC)•poly(dG-dC) upon bifunctional adduct formation by both di- and trinuclear platinum compounds.[44] The *trans*-NH_3 group of 1,1/*c*,*c* is in the equivalent position to the NH_2 group and the peaks in this region evolve over time to give a range of peaks indicative of a variety of distinct Pt–NH_3 environments. The range of ^{15}N shifts is similar to that observed for the Pt–NH_2 environments of the 1,1/*t*,*t* final product conformers and there is similar strong deshielding in the ^{1}H dimension for some of these shifts, indicative of hydrogen-bonding interactions between the *trans*-NH_3 protons and the DNA. This interpretation is also consistent with the observation of *syn* conformations of even unplatinated nucleotides in the isolated adducts of 1,1/*t*,*t* and 1,0,1/*t*,*t*,*t* with the 8-mer d(ATGTACAT)$_2$.[45,46] The *syn* conformation for purine nucleotides is a requirement for adoption of the left-handed conformation. Such interactions are not observed in the models of the bifunctional adducts in B-form DNA in which the Pt–NH_2 (1,1/*t*,*t*) or *trans*-NH_3 (1,1/*c*,*c*) protons are positioned away from the DNA with no contact with anything other than solvent. It is of interest that the structure of the cisplatin interstrand cross-link involves a localized Z-DNA structure and relies on electrostatic interactions of the phosphates with each GC base pair.[14,47,48]

Conclusion

For 1,1/*c*,*c*-en, the overall profile of bifunctional adduct formation and structure is similar to that of both 1,1/*c*,*c* and 1,1/*t*,*t*. The clinically important BBR3464 undergoes extensive decomposition in human blood with loss of the trinuclear structure, and any "second generation" polynuclear platinum clinical candidates should have similar DNA-binding profiles but be less susceptible to deactivating bridge-cleavage reactions. Both the 1,1/*c*,*c* and 1,1/*t*,*t* dinuclear geometries display in vivo antitumor activity.[6] The 1,1/*c*,*c* chelate (dach) series is a reasonable candidate for further development based on its robustness to sulfur nucleophiles[33] and its DNA-binding profile, as shown here.

Experimental Section

Chemicals: The sodium salt of the HPLC-purified oligonucleotide 5′-(ATAT**G**TACATAT)-3′ (**I**) was purchased from Geneworks. [^{15}N]Ethylenediamine was purchased as the hydrochloride salt from Isotech. The nitrate salt of the fully ^{15}N-labeled [{*cis*-PtCl($^{15}NH_3$)$_2$}$_2${μ-NH_2-$(CH_2)_6NH_2$}]$^{2+}$ ([^{15}N]1,1/*c*,*c*, [^{15}N]**1**) was prepared from *cis*-[PtCl$_2$($^{15}NH_3$)$_2$] and $AgNO_3$ by using procedures similar to those previously published.[5] The nitrate salt of fully ^{15}N-labeled [{*cis*-PtCl(en)}$_2${μ-$^{15}NH_2$-$(CH_2)_6{}^{15}NH_2$)}]$^{2+}$ (1,1/*c*,*c*-en, [^{15}N]**1-en**)[6] was prepared by an analogous procedure and characterized by ^{1}H and ^{195}Pt NMR spectroscopy and elemental analysis.

Sample preparation: For reactions with [^{15}N]**1**, stock solutions of duplex **I** were prepared as follows: the HPLC-purified oligonucleotide was first dialyzed against 0.75 mM phosphate buffer (pH 7.0, 5 L), then freeze-dried, and reconstituted in deionised H_2O (500 μL) to give stock solution A (phosphate concentration 58.5 mM). After removal of the aliquots needed for the two reactions in phosphate buffer, the remaining solution was desalted on a Sephadex G-25 column with $NaClO_4$ (24.57 mM) as the eluent, then freeze-dried, and redissolved in H_2O (400 μL) to give stock solution B (215 mM $NaClO_4$). For the reaction with [^{15}N]**1-en**, a stock solution of duplex **I** was prepared as described for stock solution B with $NaClO_4$ (20.57 mM) as eluent, then freeze-dried, and redissolved in H_2O (200 μL) to give stock solution C (360 mM $NaClO_4$). The duplex concentrations were estimated spectrophotometrically to be 4.1 (solution A), 2.0 (solution B), and 4.0 mM (solution C) based on the absorption coefficient of $\varepsilon_{260} = 186.35 \times 10^3\,M^{-1}cm^{-1}$ for these sequences derived by using the method of Kallansrud and Ward.[49]

Aquation of [^{15}N]1,1/*c*,*c*-en: The ^{15}N-labeled starting material ([^{15}N]**1-en**) (0.40 mg, 0.44 μmol) was dissolved in 15 mM $NaClO_4$ in D_2O/H_2O (5:95, 435 μL) at pH 6.79. 1,4-Dioxane (5 μL of a 10 mM solution) was added as a reference to give a total volume of 440 μL and an initial concentration of [^{15}N]**1-en** of 1.01 mM. The sample was immediately placed in the spectrometer and a series of [^{1}H,^{15}N] HSQC NMR spectra were recorded at 298 K until equilibrium conditions were obtained. The final pH of the solution was 5.0.

The kinetic analysis of the aquation reaction was undertaken by measuring the peak volumes of the peaks in the *trans*-NH_2 region of the [^{1}H,^{15}N] HSQC NMR spectra and calculating the relative concentrations of the dichloro and mono- and diaqua species at each time point in the same manner as described previously for the aquation of 1,1/*c*,*c*.[35] Full details are provided in the Supporting Information.

pK_a determination of the [^{15}N]1,1/*c*,*c*-en diaquated adduct: $AgNO_3$ (35.5 mg, 1.4 mmol) was dissolved in H_2O (1.0 mL) and a 6.95 μL (1.8 equiv) aliquot was added to [^{15}N]**1-en** (0.66 mg, 0.73 μmol) in a solution containing 2.0 M $NaClO_4$ (35 μL), D_2O (35 μL), H_2O (620 μL), and 10 mM 1,4-dioxane (10 μL, as reference). The solution was incubated overnight at 37 °C and then centrifuged to remove the AgCl precipitate. The final concentration of the 1,1/*c*,*c*-en diaquated species was 1.05 mM in $NaClO_4$ (100 mM in D_2O/H_2O (5:95)). Adjustments to pH were carried out by the addition of NaOH (0.1 or 0.01 M in D_2O/H_2O (5:95)) and $HClO_4$ (0.1 or 0.01 M in D_2O/H_2O (5:95)), respectively. ^{1}H and ^{15}N NMR spectra were recorded in the pH range 3.4–10.3.

The pH titration data were analyzed by using Equation (1), in which K_a is the acid dissociation constant for one Pt–OH_2 group of the 1,1/*c*,*c*-en diaqua complex and δ_A and δ_B are the chemical shifts of the diaqua and dihydroxo complexes, respectively. The program KaleidaGraph[50] was used for fitting.

$$\delta = (\delta_A[H^+] + \delta_B K_a)/([H^+] + K_a) \quad (1)$$

Reactions of duplex I with [^{15}N]1

Reaction in 15 mM sodium phosphate and 80 mM $NaClO_4$: Duplex **I** stock solution A (115 μL, 469.2 nmol of duplex in 58.5 mM sodium phosphate), sodium 3-trimethylsilyl[D_4]propionate (TSP; 5 μL of 10 mM), $NaClO_4$ solution (40 μL of 860 mM), D_2O (21.5 μL), and H_2O (208.5 μL) were combined and the sample was annealed by heating to 360 K and slowly cool-

 © 2008 Wiley-VCH Verlag GmbH & Co. KGaA, Weinheim

ing to room temperature. A freshly prepared solution of [^{15}N]**1** (0.34 mg, 0.4 μmol) in H_2O (40 μL) was added to this solution to give a final volume of 430 μL, with final concentrations of 1.1 mM **I** (duplex), 15 mM phosphate buffer, 80 mM $NaClO_4$, and 1.0 mM [^{15}N]**1**. A total of 10 μL of the solution was taken out for pH measurement ($pH_0 = 5.9$). The reaction at 298 K was followed by ^{1}H and [^{1}H,^{15}N] HSQC NMR spectroscopic methods until completion after approximately 8 d.

Reaction in 100 mM sodium phosphate: Duplex **I** stock solution A (128 μL, 522.2 nmol of duplex in 58.5 mM sodium phosphate), TSP (2 μL of 10 mM), sodium phosphate (26 μL of 1.401 M, pH 5.5), D_2O (21.5 μL), and H_2O (238.5 μL) were combined and the sample annealed by heating to 360 K and slowly cooling to room temperature. A freshly prepared solution of [^{15}N]**1** (0.34 mg, 0.4 μmol) in H_2O (22 μL) was added to this solution to give a final volume of 438 μL and final concentrations of 1.19 mM **I** (duplex), 100 mM phosphate buffer, and 1.0 mM [^{15}N]**1**. A total of 10 μL of the solution was removed for pH measurement ($pH_0 = 5.4$). The reaction at 298 K was followed by ^{1}H and [^{1}H,^{15}N] HSQC NMR spectroscopic methods until completion after approximately 3 weeks.

Reaction in 112 mM $NaClO_4$: Duplex **I** stock solution B (220 μL, 440 nmol of duplex in 215 mM $NaClO_4$), TSP (2 μL of 10 mM), D_2O (20 μL), and H_2O (148 μL) were combined in an NMR tube. The sample was annealed by heating to 360 K and slowly cooling to room temperature. A freshly prepared solution of [^{15}N]**1** (0.30 mg, 0.39 μmol) in H_2O (30 μL) was added to give a final volume of 420 μL and final concentrations of 1.05 mM **I** (duplex), 112 mM $NaClO_4$, and 0.95 mM [^{15}N]**1**. A total of 10 μL of the solution was removed for pH measurement ($pH_0 = 5.6$). The reaction at 298 K was followed by ^{1}H and [^{1}H,^{15}N] HSQC NMR spectroscopic methods over a total period of 3 d.

Reactions of duplex I with [^{15}N]1-en: Duplex **I** stock solution (100 μL, 398.2 nmol of duplex in 360 mM $NaClO_4$), TSP (2 μL of 10 mM), 19 μL D_2O, and 259 μL H_2O were combined and the sample was annealed by heating to 360 K and slowly cooling to room temperature. A total of 40 μL of the solution was removed for pH measurements with ≈1 M NaOH (31 μL) added to give a final $pH_0 = 5.3$. A freshly prepared solution of [^{15}N]**1-en** (0.33 mg, 0.4 μmol) in H_2O (40 μL) was added to this solution to give a final volume of 413 μL with final concentrations of 0.91 mM **I** (duplex), 100 mM $NaClO_4$, and 0.89 mM [^{15}N]**1-en**. The reaction at 298 K was followed by ^{1}H and [^{1}H,^{15}N] HSQC NMR spectroscopic methods until completion after approximately 2 d.

NMR spectroscopy: The NMR spectra were recorded on a Bruker 600 MHz spectrometer (^{1}H, 600.1 MHz; ^{15}N, 60.8 MHz) fitted with a pulsed-field gradient module and 5 mm triple resonance probehead. The ^{1}H NMR chemical shifts were internally referenced to TSP and the ^{15}N chemical shifts externally referenced to $^{15}NH_4Cl$ (1.0 M in 1.0 M HCl in 5% D_2O in H_2O). The ^{1}H NMR spectra were acquired with water suppression by using the watergate 3-9-19 pulse sequence.[51,52] The two-dimensional [^{1}H,^{15}N] heteronuclear single-quantum coherence (HSQC) NMR spectra optimized for $^1J(^{15}N,^1H) = 72$ Hz were recorded by using a standard Bruker phase-sensitive HSQC pulse sequence.[53] The ^{15}N NMR signals were decoupled by irradiating with the GARP-1 sequence at a field strength of 6.9 kHz during the acquisition time. Typically for 1D ^{1}H NMR spectra, 32 scans and 32K points were acquired by using a spectral width of 12 kHz and a relaxation delay of 2.5 s. For kinetics studies involving [^{1}H,^{15}N] HSQC NMR spectra, four transients were collected for 96 increments of t_1 (allowing spectra to be recorded on a suitable timescale for the observed reaction), with an acquisition time of 0.069 s, spectral widths of 6 kHz in f_2 (^{1}H) and 5.5 kHz in f_1 (^{15}N). 2D spectra were completed in 14 min. The 2D spectra were processed by using zero-filling up to the next power of two in both f_2 and f_1 dimensions.

All samples (including buffers, acids) were prepared so that there was a 5:95 D_2O/H_2O concentration (for deuterium lock but with minimal loss of signal as a result of deuterium exchange). Spectra were recorded at 298 K and the samples were maintained at this temperature when not immersed in the NMR probe.

The pH of the solutions was measured on a Shindengen pH Boy-P2 (su19A) pH meter and calibrated against pH buffers of pH 6.9 and 4.0. The electrode surface was placed in contact with a volume of 5.0 μL of the solution and the pH recorded. These aliquots were not returned to the bulk solution (as the electrode leaches Cl^-). Adjustments to pH were made by using 0.04, 0.2, and 1.0 M $HClO_4$ in 5% D_2O in H_2O, or 0.04, 0.2, and 1.0 M NaOH in 5% D_2O in H_2O.

Data analysis: The kinetics of the reactions of [^{15}N]**1** with duplex **I** were analyzed by measuring peak volumes in the Pt–NH_3 region of the [^{1}H,^{15}N] HSQC NMR spectra by using the Bruker XWINNMR[54] software package and calculating the relative concentrations of the various species at each time point, in the same manner as described previously for the reaction of 1,1/*t*,*t*.[26] For a given reaction, peak volumes were determined using an identical vertical scale and threshold value. The peak volume data from the *cis*-NH_3 region was used for the kinetic analyses and comparison of the time-dependent changes of peaks in the *trans*-NH_3 region was used to confirm the peak assignments. Only limited information could be obtained from the NH_2 region as the peaks for mono- and bifunctional adduct peaks lie very close to the ^1H_2O resonance.

All species, other than [^{15}N]**1**, gave rise to two NH_3 peaks in each of the *cis*- and *trans*-NH_3 regions for the nonequivalent {PtN_3Y} groups. In some cases, overlap between peaks is significant (e.g., the peaks from the non-aquated {PtN_3Cl} group of the aquachloro species **2** are coincident with the peak from **1**). For reactions in the absence of phosphate, reliable concentrations could be obtained for all species along the pathway to the formation of the bifunctional adduct (Scheme 1) because there is always one of the pairs of peaks that is free from overlap. Thus, reliable intensities (and concentrations) were obtained by doubling the volume of the discrete peaks in the *cis*-NH_3 region. The appropriate differential equations were integrated numerically and rate constants were determined by a nonlinear optimization procedure by using the program SCIENTIST.[55] The errors represent one standard deviation. In all cases the data were fitted by using the appropriate first- and second-order rate equations. The kinetic model is provided in the Supporting Information.

For the reactions in phosphate it was not possible to obtain reliable concentrations of the intermediate phosphatochloro species **5** or the phosphato monofunctional adduct **7** due to the coincidence of 1) the peaks from the {PtN_3Cl} groups in **1** and **5**, 2) the {PtN_3PO_4} groups in **5** and **7**, and 3) the peaks from the Pt–NH_3 groups bound to guanine N7 in the mono- (**3** and **7**) and bifunctional adducts. For this reason it was not possible to obtain kinetic parameters for the reactions in 15 or 100 mM phosphate, but the concentrations of species observed during the reactions were estimated based on the relative volumes of peaks in the *cis*-Pt–NH_3 region after correction for overlap (see Figure S5). It was assumed that in the early stages of the reaction the {PtN_3PO_4} peak at $\delta = 3.86/-62.5$ ppm (labeled **5d** in Figure 1b) was derived only from the phosphatochloro species **5**, so that the approximate concentration of **1** could be derived from the {PtN_3Cl} peak ($\delta = 3.78/-65.9$ ppm) after correcting for the overlap of **2** and **5**. When no dichloro species remained the concentration of the phosphato monofunctional adduct **7** was derived from the difference in the intensity of the {PtN_3PO_4} ($\delta = 3.86/-62.5$ ppm) and {PtN_3Cl} ($\delta = 3.78/-65.9$ ppm) peaks. The concentration of the bifunctional adduct was estimated from the total broad peaks at $\delta \approx 4.2/-60$ ppm after adjusting for the overlap of the N7G bound ends of the monofunctional adducts **3** and **7**.

Molecular modeling: Molecular models of mono- and bifunctional adducts of **1** bound to 5′-d(ATAT**G**TACATAT)$_2$ (**I**) were generated and subjected to molecular dynamics simulations by using Amber 9.[56] The partial atomic charges for both the mono- and bifunctionally bound **1** were derived from DFT calculations performed by using the Amsterdam Density Functional (ADF) program.[57–59] Calculations on the 1,1/*c*,*c* complex were undertaken with one or two chloro ligands removed, with formal molecular charges of 3+ and 4+, respectively. A scalar ZORA relativistic basis set was employed to accommodate the high molecular weight platinum atoms of **1**. This particular approach restricts the core electrons to the full 4d orbital on platinum, while considering the full electronic configuration of the lighter atoms.

The 1,1/*c*,*c* complex was manually docked in a variety of mono- or bifunctional binding arrangements followed by coarse minimization of the platinum complex to eliminate any possible clashes within the adduct. Equilibration of the systems was performed over 220 ps. One each of the mono- and bifunctional systems was then subjected to a 10 ns molecular

 © 2008 Wiley-VCH Verlag GmbH & Co. KGaA, Weinheim

dynamics production simulation. All simulations were performed by using the 2002 Amber force field modified with parameters developed for the 1,1/*c*,*c* complex[60,61] under periodic boundary conditions in an octahedral water box on an SGI Altix computer provided by the Australian Partnership for Advanced Computing (APAC) at the Australian National University. Analysis of the trajectory was performed by using 3DNA[62] and images extracted from the molecular dynamics simulation were generated by using Swiss PDB Viewer 3.7 SP5[63] and rendered in POV-Ray 3.5.[64]

Acknowledgements

This work was supported by the Australian Research Council (Discovery grant to S.J.B.-P. and N.F.), the National Institutes of Health (RO1-CA78754), the National Science Foundation (INT-9805552 and CHE-9615727) and the American Cancer Society (RPG89-002-11-CDD). We thank the Australian Partnership for Advanced Computing (APAC) and IVEC for access to the computing resources used in this work and Dr. L. Byrne for assistance with NMR spectroscopy experiments.

[1] N. Farrell, *Met. Ions Biol. Syst.* **2004**, *42*, 251–296.
[2] N. Farrell, *Comments Inorg. Chem.* **1995**, *16*, 373–389.
[3] N. Farrell, Y. Qu, M. P. Hacker, *J. Med. Chem.* **1990**, *33*, 2179–2184.
[4] A. J. Kraker, J. D. Hoeschele, W. L. Elliott, H. D. H. Showalter, A. D. Sercel, N. P. Farrell, *J. Med. Chem.* **1992**, *35*, 4526–4532.
[5] N. Farrell, T. G. Appleton, Y. Qu, J. D. Roberts, A. P. S. Fontes, K. A. Skov, P. Wu, Y. Zou, *Biochemistry* **1995**, *34*, 15480–15486.
[6] N. Farrell, Y. Qu, U. Bierbach, M. Valsecchi, E. Menta in *Cisplatin: Chemistry and Biochemistry of a Leading Anticancer Drug* (Ed.: B. Lippert), Wiley-VCH, Zurich, **1999**, pp. 479–496.
[7] G. Pratesi, P. Perego, D. Polizzi, S. C. Righetti, R. Supino, C. Caserini, C. Manzotti, F. C. Giuliani, G. Pezzoni, S. Tognella, S. Spinelli, N. Farrell, F. Zunino, *Br. J. Cancer* **1999**, *80*, 1912–1919.
[8] P. Perego, C. Caserini, L. Gatti, N. Carenini, S. Romanelli, R. Supino, D. Colangelo, I. Viano, R. Leone, S. Spinelli, G. Pezzoni, C. Manzotti, N. Farrell, F. Zunino, *Mol. Pharmacol.* **1999**, *55*, 528–534.
[9] A. H. Calvert, H. Thomas, N. Colombo, M. Gore, H. Earl, L. Sena, G. Camboni, P. Liati, C. Sessa, *Eur. J. Cancer* **2001**, *37 (Supp6)*, Poster Discussion 965.
[10] J. Zehnulova, J. Kasparkova, N. Farrell, V. Brabec, *J. Biol. Chem.* **2001**, *276*, 22191–22199.
[11] V. Brabec, J. Kaspárková, O. Vrána, O. Nováková, J. W. Cox, Y. Qu, N. Farrell, *Biochemistry* **1999**, *38*, 6781–6790.
[12] M. B. G. Kloster, J. C. Hannis, D. C. Muddiman, N. Farrell, *Biochemistry* **1999**, *38*, 14731–14737.
[13] J. Kaspárková, O. Nováková, O. Vrána, N. Farrell, V. Brabec, *Biochemistry* **1999**, *38*, 10997–11005.
[14] S. R. Rajski, R. M. Williams, *Chem. Rev.* **1998**, *98*, 2723–2795.
[15] P. J. McHugh, V. J. Spanswick, J. A. Hartley, *The Lancet Oncology* **2001**, *2*, 483–490.
[16] M. L. Dronkert, R. Kanaar, *Mutat. Res.* **2001**, *486*, 217–247.
[17] E. Reed, *Clin. Cancer Res.* **2005**, *11*, 6100–6102.
[18] E. Reed, *Cancer Treat. Rev.* **1998**, *24*, 331–344.
[19] Y. Jung, S. J. Lippard, *Chem. Rev.* **2007**, *107*, 1387–1407.
[20] V. Brabec, *Prog. Nucleic Acid Res. Mol. Biol.* **2002**, *71*, 1–68.
[21] J. G. Moggs, D. E. Szymkowski, M. Yamada, P. Karran, R. D. Wood, *Nucleic Acids Res.* **1997**, *25*, 480–491.
[22] J.-C. Huang, D. B. Zamble, J. T. Reardon, S. J. Lippard, A. Sancar, *Proc. Natl. Acad. Sci. U.S.A.* **1994**, *91*, 10394–10398.
[23] D. B. Zamble, D. Mu, J. T. Reardon, A. Sancar, S. J. Lippard, *Biochemistry* **1996**, *35*, 10004–10013.
[24] J. Kasparkova, J. Zehnulova, N. Farrell, V. Brabec, *J. Biol. Chem.* **2002**, *277*, 48076–48086.
[25] S. J. Berners-Price, L. Ronconi, P. J. Sadler, *Prog. Nucl. Magn. Reson. Spectrosc.* **2006**, *49*, 65–98.
[26] J. W. Cox, S. J. Berners-Price, M. S. Davies, Y. Qu, N. Farrell, *J. Am. Chem. Soc.* **2001**, *123*, 1316–1326.
[27] S. J. Berners-Price, M. S. Davies, J. W. Cox, D. S. Thomas, N. Farrell, *Chem. Eur. J.* **2003**, *9*, 713–725.
[28] A. Hegmans, S. J. Berners-Price, M. S. Davies, D. S. Thomas, A. S. Humphreys, N. Farrell, *J. Am. Chem. Soc.* **2004**, *126*, 2166–2180.
[29] M. E. Oehlsen, Y. Qu, N. Farrell, *Inorg. Chem.* **2003**, *42*, 5498–5506.
[30] M. E. Oehlsen, A. Hegmans, Y. Qu, N. Farrell, *J. Biol. Inorg. Chem.* **2005**, *10*, 433–442.
[31] V. Vacchina, L. Torti, C. Allievi, R. Lobinski, *J. Anal. At. Spectrom.* **2003**, *18*, 884–890.
[32] M. E. Oehlsen, A. Hegmans, Y. Qu, N. Farrell, *Inorg. Chem.* **2005**, *44*, 3004–3006.
[33] J. W. Williams, Y. Qu, G. H. Bulluss, E. Alvorado, N. P. Farrell, *Inorg. Chem.* **2007**, *46*, 5820–5822.
[34] G. V. Kalayda, G. Zhang, T. Abraham, H. J. Tanke, J. Reedijk, *J. Med. Chem.* **2005**, *48*, 5191–5202.
[35] J. Zhang, D. S. Thomas, M. S. Davies, S. J. Berners-Price, N. Farrell, *J. Biol. Inorg. Chem.* **2005**, *10*, 652–666.
[36] M. S. Davies, J. W. Cox, S. J. Berners-Price, W. Barklage, Y. Qu, N. Farrell, *Inorg. Chem.* **2000**, *39*, 1710–1715.
[37] Owing to practical limitations a higher ionic strength is used here than in the previous studies of 1,1/*t*,*t* (see ref. [26]) and 1,0,1/*t*,*t*,*t* (see ref. [28]). In an initial study, [^{15}N]**1** was allowed to react with duplex **I** under similar conditions (15 mM phosphate, pH 5.2) to those used previously. This sample contained sodium acetate as an artifact of HPLC purification (an insignificant contaminant in previous reactions) and the [^{1}H,^{15}N] spectra showed ^{1}H/^{15}N peaks for both acetate- and phosphate-bound species (assignments from ref. [35]). After dialysis to remove the acetate, the addition of $NaClO_4$ (80 mM) was required to form a stable duplex at 298 K.
[38] R. C. Todd, K. S. Lovejoy, S. J. Lippard, *J. Am. Chem. Soc.* **2007**, *129*, 6370–6371.
[39] A. S. Snygg, M. Brindell, G. Stochel, S. K. C. Elmroth, *Dalton Trans.* **2005**, 1221–1227.
[40] J. Kjellstrom, S. K. C. Elmroth, *Inorg. Chem.* **1999**, *38*, 6193–6199.
[41] M. S. Davies, S. J. Berners-Price, T. W. Hambley, *Inorg. Chem.* **2000**, *39*, 5603–5613.
[42] S. Komeda, T. Moulaei, K. K. Woods, M. Chikuma, N. P. Farrell, L. D. Williams, *J. Am. Chem. Soc.* **2006**, *128*, 16092–16103.
[43] N. Farrell, *Adv. DNA Sequence-Specific Agents* **1996**, *2*, 187–216.
[44] T. D. McGregor, W. Bousfield, Y. Qu, N. Farrell, *J. Inorg. Biochem.* **2002**, *91*, 212–219.
[45] Y. Qu, N. J. Scarsdale, M.-C. Tran, N. P. Farrell, *J. Biol. Inorg. Chem.* **2003**, *8*, 19–28.
[46] Y. Qu, N. J. Scarsdale, M.-C. Tran, N. Farrell, *J. Inorg. Biochem.* **2004**, *98*, 1585–1590.
[47] H. Huang, L. Zhu, B. R. Reid, G. P. Drobny, P. B. Hopkins, *Science* **1995**, *270*, 1842–1845.
[48] F. Coste, J.-M. Malinge, L. Serre, W. Shepard, M. Roth, M. Leng, C. Zelwer, *Nucleic Acids Res.* **1999**, *27*, 1837–1846.
[49] G. Kallansrud, B. Ward, *Anal. Biochem.* **1996**, *236*, 134–138.
[50] KaleidaGraph v3.5 for Windows, Synergy Software, Reading, PA (USA).
[51] M. Piotto, V. Saudek, V. Sklenar, *J. Biomol. NMR* **1992**, *2*, 661–665.
[52] V. Sklenar, M. Piotto, R. Leppik, V. Saudek, *J. Magn. Reson. Ser. A* **1993**, *102*, 241–245.
[53] A. G. Palmer III, J. Cavanagh, P. E. Wright, M. Rance, *J. Magn. Reson.* **1991**, *93*, 151–170.
[54] XWINNMR v3.5, Bruker.
[55] SCIENTIST, Version 2.0, MicroMath, Salt Lake City.
[56] Amber 9, Assisted Model Building with Energy Refinement, D. A. Case, T. A. Darden, T. E. Cheatham III, C. L. Simmerling, J. Wang, R. Duke, R. Lou, K. M. Merz, D. A. Pearlman, M. Crowley, R. C. Walker, W. Zhang, B. Wang, S. Hayik, A. Roitberg, G. Seabra, K. F. Wong, F. Paesani, X. Wu, S. Brozell, V. Tsui, H. Gohlke, L. Yang, C. Tan, J. Mongan, V. Hornak, G. Cui, P. Beroza, D. H. Mathews, W. S. Schafmeister, W. S. Ross, P. A. Kollman, University of California, San Francisco, CA, **2006**.

 © 2008 Wiley-VCH Verlag GmbH & Co. KGaA, Weinheim

[57] C. Fonseca Guerra, J. G. Snijders, G. te Velde, E. J. Baerends, *Theor. Chem. Acc.* **1998**, *99*, 391–403.
[58] G. te Velde, F. M. Bickelhaupt, E. J. Baerends, C. Fonseca Guerra, S. J. A. van Gisbergen, J. G. Snijders, T. Ziegler, *J. Comput. Chem.* **2001**, *22*, 931–967.
[59] Amsterdam Density Functional, ADF2006, SCM, E. J. Baerends, J. Autschbach, A. Bérces, F. M. Bickelhaupt, C. Bo, P. M. Boerrigter, L. Cavallo, D. P. Chong, L. Deng, R. M. Dickson, D. E. Ellis, M. van Faassen, L. Fan, T. H. Fischer, C. Fonseca Guerra, S. J. A. van Gisbergen, J. A. Groeneveld, O. V. Gritsenko, M. Grüning, F. E. Harris, P. van den Hoek, C. R. Jacob, H. Jacobsen, L. Jensen, G. van Kessel, F. Kootstra, E. van Lenthe, D. A. McCormack, A. Michalak, J. Neugebauer, V. P. Osinga, S. Patchkovskii, P. H. T. Philipsen, D. Post, C. C. Pye, W. Ravenek, P. Ros, P. R. T. Schipper, G. Schreckenbach, J. G. Snijders, M. Solà, M. Swart, D. Swerhone, G. te Velde, P. Vernooijs, L. Versluis, L. Visscher, O. Visser, F. Wang, T. A. Wesolowski, E. van Wezenbeek, G. Wiesenekker, S. K. Wolff, T. K. Woo, A. L. Yakovlev, T. Ziegler, Vrije Universiteit Amsterdam, Amsterdam (The Netherlands), **2006**.
[60] S. Yao, J. P. Plastaras, L. G. Marzilli, *Inorg. Chem.* **1994**, *33*, 6061–6077.
[61] D. S. Thomas, Ph. D. Thesis, The University of Western Australia (Australia), **2006**.
[62] X.-J. Lu, Z. Shakked, W. K. Olson, *J. Mol. Biol.* **2000**, *300*, 819–840.
[63] N. Guex, M. C. Peitsch, *Electrophoresis* **1997**, *18*, 2714–2723.
[64] C. Cason, POV-Ray rendering engine for Windows v3.5, http://www.povray.org/.

Received: March 6, 2008
Published online: June 9, 2008

 © 2008 Wiley-VCH Verlag GmbH & Co. KGaA, Weinheim